


REGULAR PAPER

Effects of backpressure on unstart and restart characteristics of a supersonic inlet

K. Wang¹, J.Y. Wang², H.X. Huang¹, L.R. Xie¹, Y. Liu³ and H.J. Tan¹

¹College of Energy and Power Engineering, Jiangsu Province Key Laboratory of Aerospace Power System, Nanjing University of Aeronautics and Astronautics, Nanjing, China, ²School of Aeronautics and Astronautics, Sun Yat-sen University, Guangzhou, China and ³Chinese Flight Test Establishment, Xian, China

Corresponding author: K. Wang; Email: kunwang@nuaa.edu.cn

Received: 7 June 2022; **Revised:** 3 February 2023; **Accepted:** 15 February 2023

Keywords: Supersonic inlet; Backpressure; Unstart; Restart; Numerical simulation

Abstract

The unstart phenomenon of supersonic inlets caused by backpressure is dangerous for aircraft during flights because it severely reduces the air mass flow rate through the engine. We used unsteady numerical simulations to evaluate the unstart and restart characteristics of a two-dimensional supersonic inlet during rapid backpressure changes. The effects of the depressurisation time and depressurisation value on the inlet flow characteristics and restart features are discussed. The results show that the depressurisation time affects the restart procedure when the back pressure drops from the inlet unstart value to the normal working state value. When the depressurisation time decreases, it becomes easier for the inlet to restart. However, the inlet cannot restart if the depressurisation time is too long. When the depressurisation time and value were large enough, a short buzz period occurred before the inlet restarted. Both the time and value of depressurisation affected the restart characteristics.

Nomenclature

H_{th}	height of inlet throat, mm
Δt	time step, s
u_{max}	maximum velocity, m/s
Δx	cell's characteristic length, mm
CFL	Courant–Friedrichs–Lewy number
c	speed of sound, m/s
P_o	static of freestream, Pa
P_b	backpressure, Pa
t	time moment, s
f	frequency, Hz
Ma	Mach number
L	length, mm

Subscripts

0	of freestream
1	of freestream
b	at the inlet exit
th	at the inlet throat

1.0 Introduction

A supersonic inlet is a key component of a ramjet that captures and compresses air for the combustor at the desired airflow quality. Failure to start the inlet can lead to serious problems during the flight. Once the supersonic inlet undergoes unstart, there is a sharp decrease in the flow rate, total pressure recovery coefficient, and thrust. Moreover, the inlet unstart is likely to cause a combustor flameout that could destroy the whole engine structure [1]. Therefore, it is essential to avoid the inlet unstart phenomenon. Two major factors cause inlet unstart: the high internal contraction ratio and the abrupt increase in the downstream backpressure (which always happens as the required flow rate of the engine decreases).

Multiple experimental and numerical studies have investigated the inlet unstart characteristics caused by high backpressure. Saied Emami et al. [2] experimentally studied the unstart and restart process of inlets caused by backpressure variations for the flow with the Mach number of 4.0. They obtained the range of contractions for a successful ratio. Van Wie [3] reviewed the datasets in the literature and presented empirical curves of the limiting contraction ratios versus the different inlet conditions. The inlets with a high contraction ratio tended to exhibit “hard” unstart phenomena with considerable pressure losses in the combustor. However, “soft” unstarts occurred for inlets with low contraction ratios, where the unstart phenomenon occurred as flow mass venting [4]. Researchers have reported transient propagation unstart velocities of 26m/s [5] and 55 to 70m/s [4]. The highly violent oscillatory mode of unstart resulted from approximately 124Hz [5]. Maye and Paynter [6, 7] developed an Euler analysis procedure for predicting the unstart tolerance of supersonic inlets. Trapier et al. [8–10] combined the experimental and computational approaches to perform a detailed analysis of the oscillations of inlet buzz shock waves. The algorithms for cumulative sum algorithms and the generalised likelihood ratio were applied to the unstart warning. The same algorithms were also used by Li et al. [11]. Lee et al. [12] investigated the flow characteristics for rectangular and axisymmetric supersonic inlets and reported that the base frequencies for both models were at similar levels during the continuous buzz. Wooram [13] computationally examined the hysteretic inlet buzz under various mass flow conditions and explained hysteretic buzz and buzz transition mechanisms. Xie [14] investigated the restart performance of a mixed-compression supersonic inlet under the unstart condition caused by raising the backpressure. The hysteresis was eliminated by a pneumatic throat formed by shock wave–boundary layer interactions. Chen [15] reported that the moment of the port cover had a great influence on the inlet starting performance, and opening the port cover during inflation was conducive to inlet starting.

The inlet unstart state is usually accompanied by strong unsteady characteristics, such as remarkable shock wave motions and pressure fluctuations throughout the inlet channel. Previous studies have mainly focused on the influence of downstream mass flow choking and regular backpressure variations on the inlet start performance [14, 16, 17]; however, most of these studies have ignored the impact of instantaneous high pressure within the downstream combustion chamber. It is very difficult for traditional backpressure simulation methods based on the mechanical blockage technique, such as a plug or a flap, to simulate the short-time pressurisation. Therefore, an unsteady numerical simulation technique was used to analyse the inlet start and unstart phenomena caused by sudden backpressure changes from the combustion chamber. Then, the unsteady flow field characteristics were explored.

2.0 Computational methods

2.1 Inlet geometry

Figure 1 shows the typical two-dimensional supersonic inlet model. External compression was achieved by three ramps inclined to the freestream direction by 8.5° , 16.5° and 25.5° . The internal surface of the cowl lip was inclined at 12.5° to the freestream direction. The inlet throat height is expressed as H_{th} , and H_{th} dimensionalises other geometrical parameters of the inlet. The length and offset ratios of the diffuser were $9.4H_{th}$ and $0.79H_{th}$, respectively; there was abrupt turning at the exit. The self-starting and designed Mach numbers of the inlet were 2.4 and 3.3. Table 1 shows the freestream conditions.

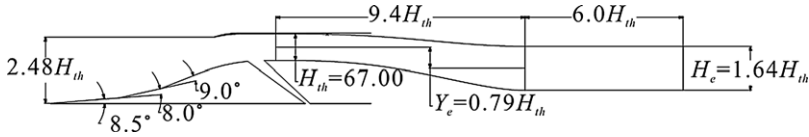


Figure 1. Model of the inlet.

2.2 Numerical approach

The commercial CFD software ANSYS Fluent was employed for the numerical calculations. Fluent solves the Reynolds-averaged Navier–Stokes equations in a finite-volume framework. As the flow velocity in the test is relatively high, the compressible density-based flow solver is selected. The N-S equations are discretised by a second-order upwind scheme and the turbulent viscosity is resolved by the $k-\omega$ shear stress transport turbulent model. Roe's method was used as the inviscid flux scheme. The simulated fluids were treated as a compressible ideal gas with standard air composition. The Sutherland's formulation was adopted to calculate the molecular viscosity of the gas. The pressure far-field and pressure-outlet boundary conditions were applied, and a nonslip adiabatic boundary condition was employed for all the wall surfaces. The backpressure variations were implemented by a user-defined function. Unsteady calculations were based on the flow fields obtained from the initial steady calculation.

2.2.1 Simulation validation

To demonstrate the reliability of the computational fluid dynamics (CFD) data, we validated the turbulent model and the numerical methods introduced in the previous section against the existing experimental data published in the literature that dealt with the buzz problems in the supersonic axisymmetric inlet [18]. The Mach number was 2; the Reynold number was approximately 10^7 , and the reference length of the inlet diameter was 60mm. We chose the second example for the simulation in which the throttle ratio was 0.67. Figure 2(a) gives the static pressure histories of the experimental and numerical methods at the P7 station. Figure 2(b) gives the flowfield schlieren measured during the test and those obtained by computations. The numerical results of the pressure histories and shock wave structures demonstrate good consistency with the experimental results.

2.2.2 Grid-sensitivity analysis

It is important and necessary to ensure that the obtained CFD results are grid-independent. Three sets of grids with various densities (grid 1 = 1.1×10^5 ; grid 2 = 1.7×10^5 , grid 3 = 2.5×10^5) were used. Figure 3 shows the results obtained with different meshes. There are slight differences between the grid 2 and the grid 3 results, which proves the grid independence. However, the grid 1 shows a large deviation. Therefore, grid 2 was chosen for numerical investigations in this paper. To fulfill the mesh quality requirements of the near-wall models used to resolve the flows, we used the dimensionless distance y^+ of the wall-adjacent nodes, which was approximately 1.0.

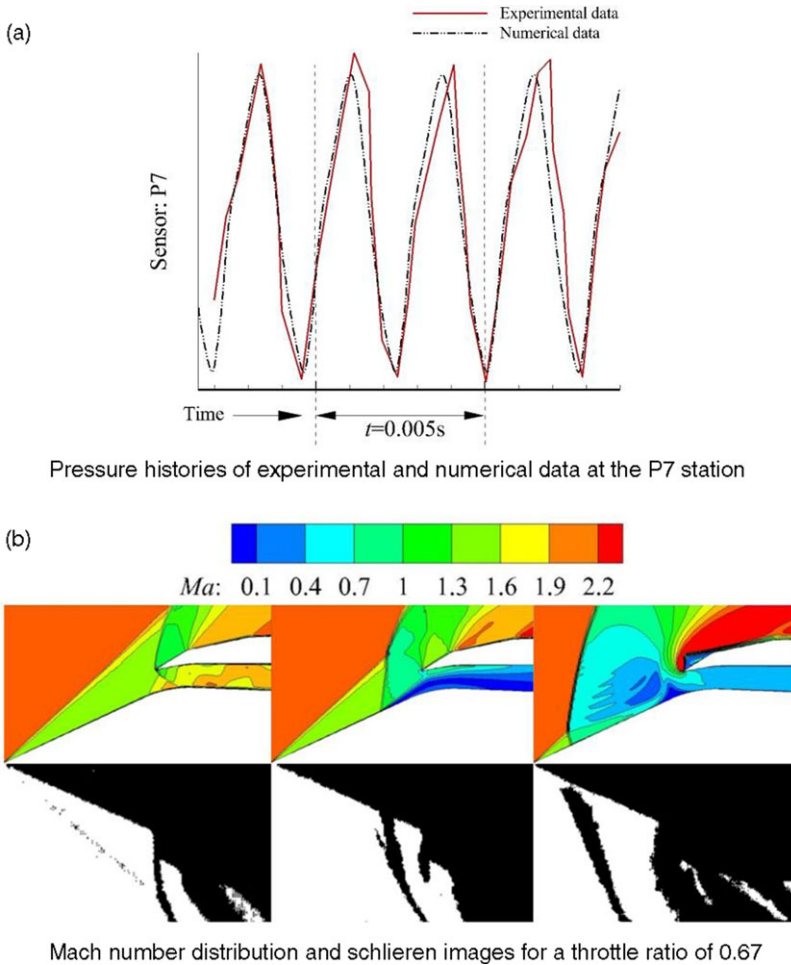
2.2.3 Time step sensitivity analysis

In an unsteady computational domain, the size of the time step directly affects the accuracy of the calculation. Therefore, it is essential to select an appropriate time step size that can resolve the flow domain. The time step is estimated by the following equation [19]:

$$\Delta t = \frac{\Delta x}{(c + u_{\max})} CFL, \quad (1)$$

Table 1. Freestream conditions for simulation

Mach number	Static temperature (K)	Static pressure (Pa)
2.4	223.25	54048
3.3	216.65	5529.3



Pressure histories of experimental and numerical data at the P7 station

Mach number distribution and schlieren images for a throttle ratio of 0.67

Figure 2. Pressure distribution and flow structure.

where Δx is the cell's characteristic length, and u_{\max} is the maximum velocity in the flow field. CFL , which is the Courant–Friedrichs–Lewy number, equals 0.6. According to [1], the time step is 1×10^{-6} s. To assess the step sensitivity in this paper, we evaluated three sequences of grid sizes, namely, 5×10^{-6} s, 1×10^{-6} s and 5×10^{-7} s. The implicit time discretisation method is adopted, and 200 steps are iterated within a single time step to ensure the convergence of the transient flow field at each time step. Figure 4 shows the flow histories of the throat calculated under different step times. All the time step sizes show a similar trend; however, the results of the 1×10^{-6} s and 5×10^{-7} s sizes were almost the same. The results become step non-sensitive when the step size of 1×10^{-6} s is chosen.

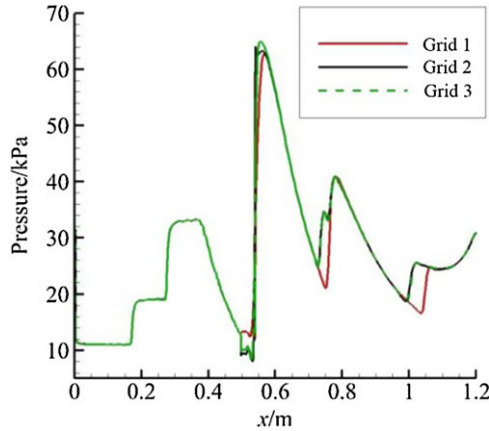


Figure 3. Pressure distribution on the ramp and the diffuser surface.

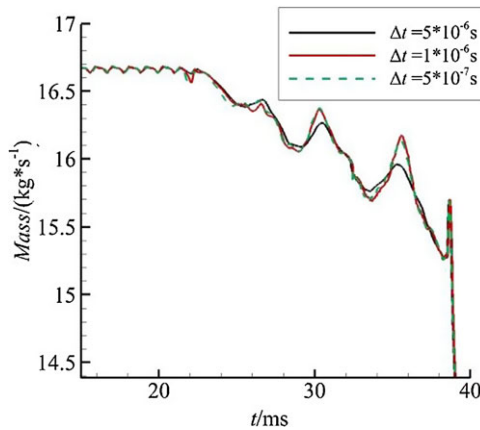


Figure 4. Throat flow history calculated under different step time.

3.0 Results and discussion

3.1 Unstart and restart characteristics of an inlet under the design condition

To examine the effects of the depressurisation time and value on the inlet unstart and restart characteristics under the design condition, we performed simulations with eight backpressure variation modes (see Table 2) with $P_0 = 5529.3\text{Pa}$. The simulations initially started from $P_b = 24P_0$ at which the inlet was under normal operating conditions. The backpressure was increased to $32P_0$ within 40ms until the inlet switched to a typical unstart state. Then, seven kinds of depressurisations were simulated.

3.1.1 Unstart flow field under rapid pressurisation

To obtain a typical unstart flow field, we conducted an unsteady simulation based on backpressure ranging from $24P_0$ to $32P_0$ within 40ms. The backpressure increased linearly with time for simplifying the pressurisation process, as follows:

$$P_b = P_0 * (24 + 200 * t) . \tag{2}$$

The throat flow history under the pressurisation process is presented in Fig. 5. From Fig. 5, it is clear that the unstart process can be divided into three stages: AB, BC and CD. Figures 6 and 7 show the

Table 2. Backpressure change mode under design conditions

Case	Mach number	Initial value (Pa)	End value (Pa)	Time (ms)	State
1	3.3	$24P_0$	$32P_0$	40	Unstart
2	3.3	$32P_0$	$24P_0$	0	Restart
3	3.3	$32P_0$	$24P_0$	5	Restart
4	3.3	$32P_0$	$24P_0$	10	Buzz
5	3.3	$32P_0$	$16P_0$	10	Restart
6	3.3	$32P_0$	$16P_0$	20	Buzz
7	3.3	$32P_0$	$13P_0$	23.75	Buzz
8	3.3	$32P_0$	$8P_0$	30	Restart

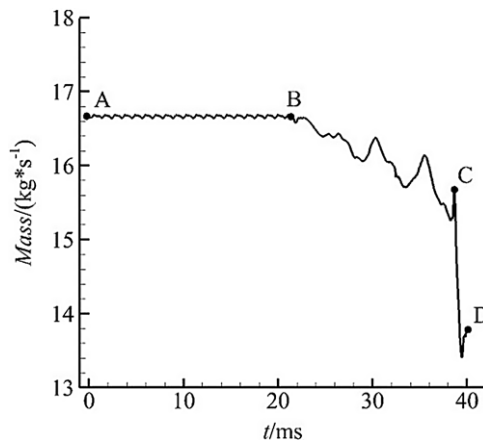


Figure 5. Throat flow history of Case 1.

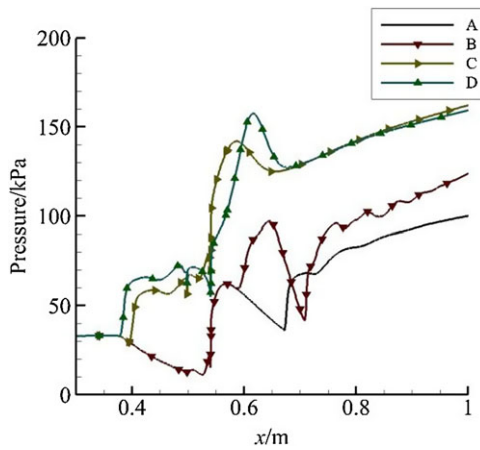


Figure 6. Pressure distributions of the ramp wall at the A, B, C, and D moments time points.

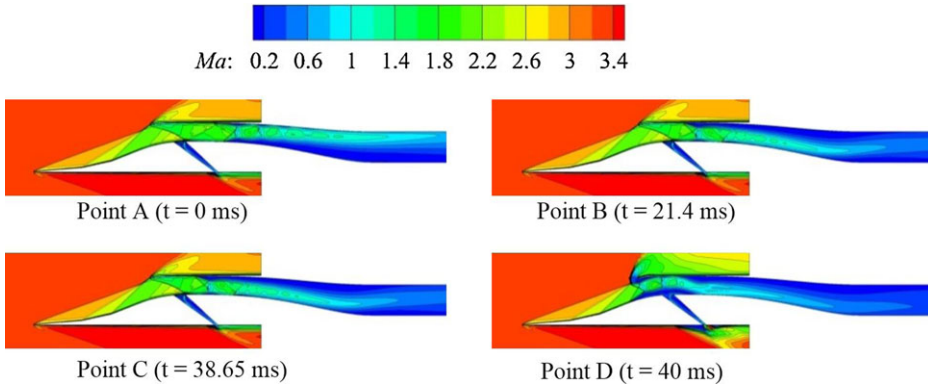


Figure 7. Mach number contours of the inlet.

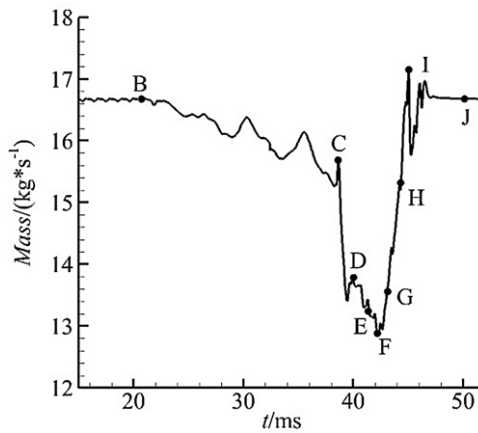


Figure 8. Throat flow history of Case 2.

pressure distributions of the ramp wall and the Mach number contours of the inlet at the four moments A, B, C and D. Using the results in Figs. 5–7, we describe the flow characteristics of the unstart process.

Initially, the inlet works in the supercritical state in the AB stage. The first shock wave is located downstream of the throat, and the throat flow is constant. The first shock wave is pushed through the throat as the backpressure increases. The throat flow decreases slightly under the combined action of the airflow separation on the ramp wall and the cavity. After the C moment (see Fig. 5), the first shock wave is pushed out of the lip and appears as an X-shaped wave. Airflow spillage occurs at the lip, and the throat flow decreases rapidly. The typical unstart flow field is established.

3.1.2 Effects of depressurisation time on restart

Based on the simulated unstart flow field in the last section, we investigated the influence of different depressurisation speeds on inlet restart characteristics. The depressurisation process was also linear.

Figures 8–11. show the throat flow histories of Cases 2 and 3; they also show the Mach number contours of the inlet at different moments. The two kinds of throat flow histories show that the flow begins to rise (stage FI) after a period of decline (stage DF), and the inlet finally restarts. The throat flow histories of the two depressurisation methods are almost similar. However, the flow decline (stage DF) and the time of flow recovery (stage FI) in Case 3 were greater than those in Case 2. The minimum

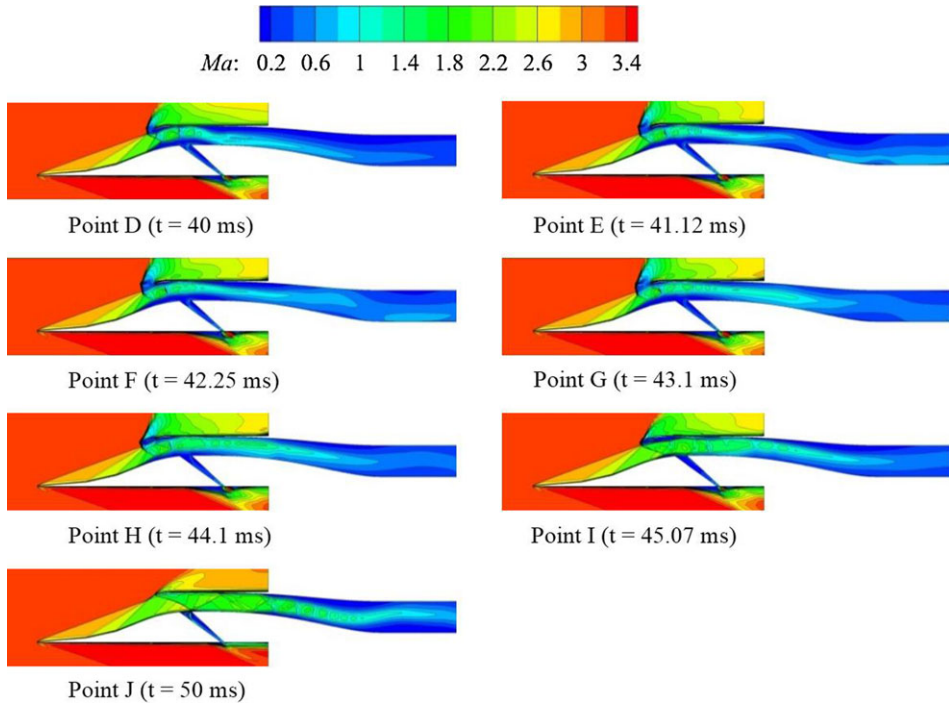


Figure 9. Mach number contours of the typical moments of Case 2.

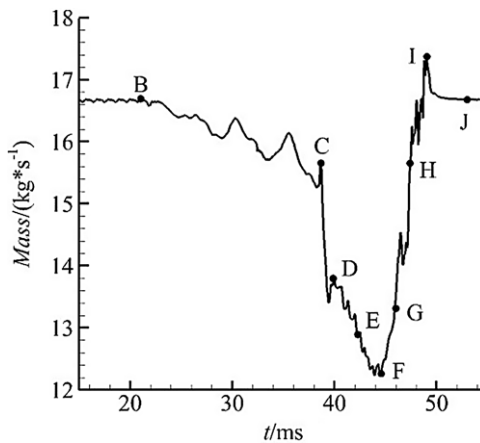


Figure 10. Throat flow history of Case 3.

throat flow in Case 3 was smaller than that in Case 2. This took more time to propagate the downstream pressure signal to upstream in Case 3.

According to the Mach number contours, the flow fields of the inlet restart process were approximately the same for the two cases. The detached shock and the airflow separation on the external contraction surface moved upstream from the D moment to the F moment moved upstream because of the high pressure. At the F moment, the shock wave was located at the upstream position. Then, the lower pressure signal reached upstream. Simultaneously, the detached shock wave moved downstream, and

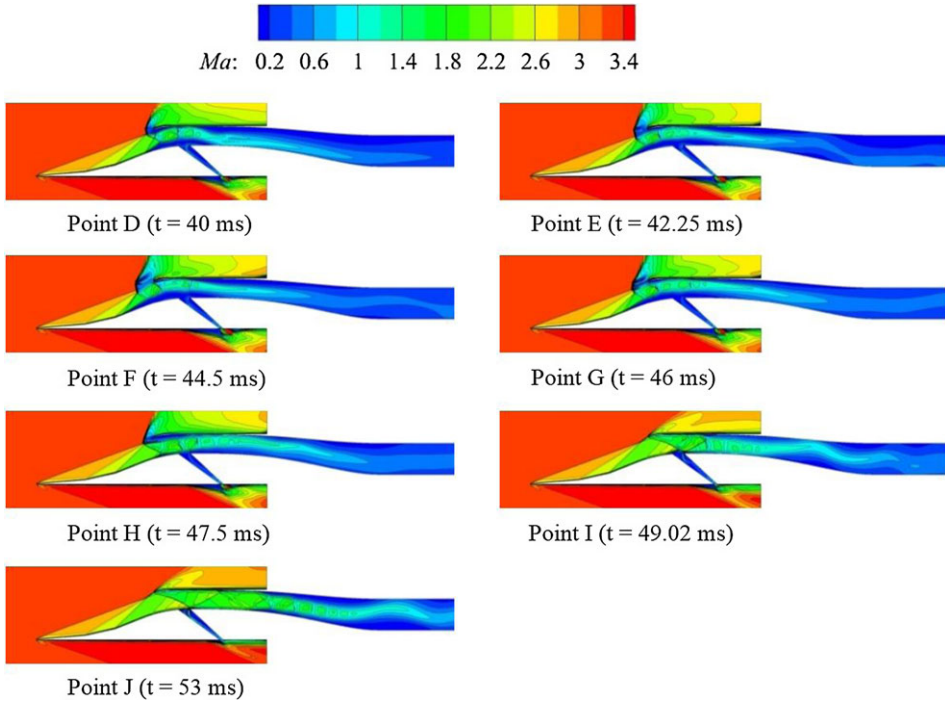


Figure 11. Mach number contours of the typical moments of Case 3.

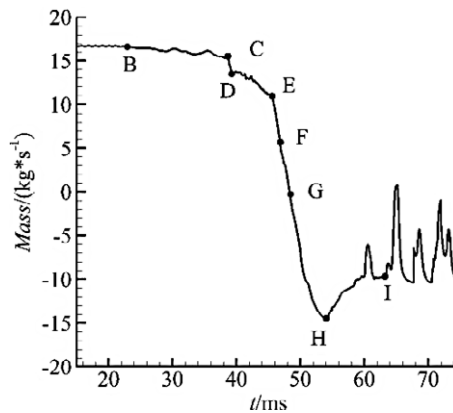


Figure 12. Throat flow history of Case 4.

the separation bubble shrank; the entering airflow rate also increased. Finally, the external compression shock system was reestablished, and the inlet restarted.

Figure 12 shows the throat flow history of Case 4. Clearly, the inlet remains in the unstart state even if the backpressure drops to normal working conditions. From the Mach number contours in Fig. 13, the flow patterns can be divided into four stages: DE, EG, GH and HI.

The DE stage of Case 4 is similar to the DF stage of Case 3, except that the airflow spillage is larger for the DE stage. After the E moment, the shock wave at the internal contraction section is pushed out of the lip, and the separation bubble moves forward to the second compression surface. At the G moment, the throat flow decreases to zero, and the separation bubble occupies most of the inlet entrance. Then,

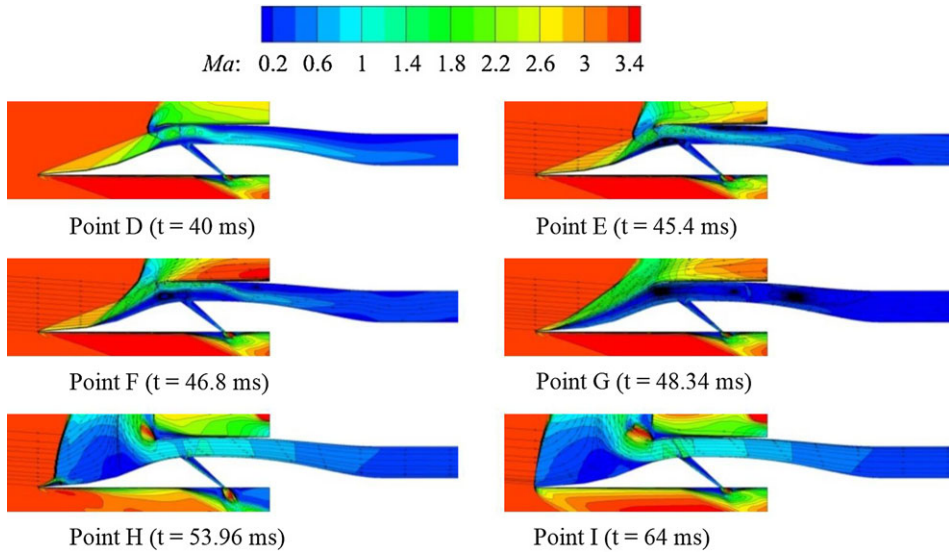


Figure 13. Mach number contours of the typical moments of Case 4.

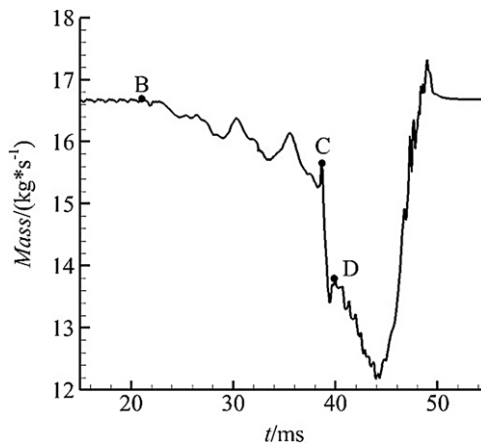


Figure 14. Throat flow history of Case 5.

the backpressure is close to the ending value of $24P_0$, greater than the pressurisation value from the normal shock. Consequently, a reverse flow forms, and the buzz starts.

Our discussions clearly show that the backpressure drops from the inlet unstart value to the normal working value. The inlet becomes easier to restart with the decrease in the depressurisation time. However, the inlet cannot restart if the depressurisation time is too long. The depressurisation time by fuel reduction in the combustion chamber will not be as short as the setting value of 5ms. Therefore, different depressurisation values were specified to study the restart characteristics, as shown in Cases 5–8 in Table 2.

3.1.3 Effects of depressurisation value on the restart

Figures 14–15 show the throat flow histories of Cases 5 and 6. The inlet can restart when the depressurisation time is 10ms; however, it stays in the unstart state when it is 20ms. A comparison of Cases 5

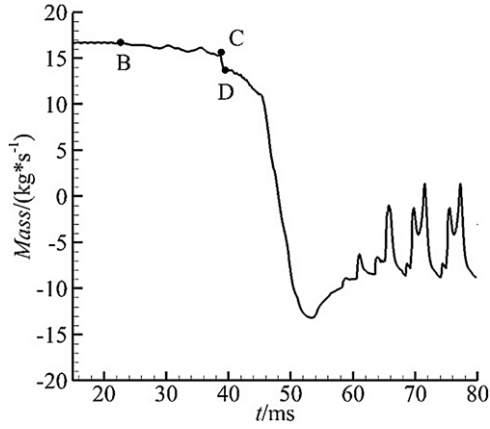


Figure 15. Throat flow history of Case 6.

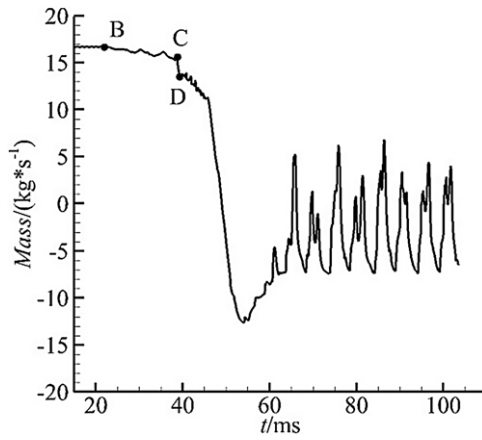


Figure 16. Throat flow history of Case 7.

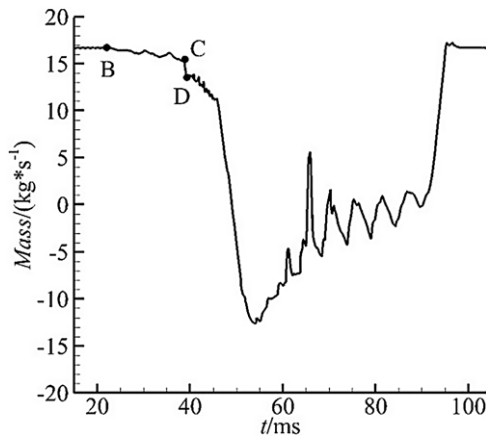


Figure 17. Throat flow history of Case 8.

Table 3. Backpressure change modes under start condition

Case	Mach number	Initial value (Pa)	End value (Pa)	Time (ms)	State
9	2.4	$11P_0$	$13P_0$	20	Unstart
10	2.4	$13P_0$	$11P_0$	10	Restart
11	2.4	$13P_0$	$11P_0$	20	Buzz
12	2.4	$13P_0$	$7P_0$	30	Buzz
13	2.4	$13P_0$	$5P_0$	40	Restart

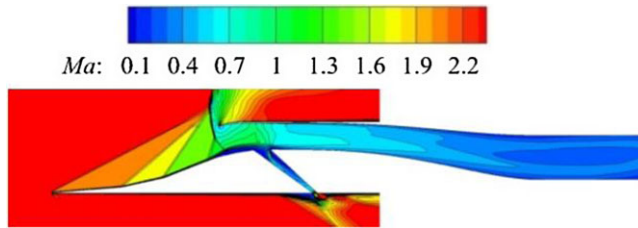


Figure 18. Typical unstart Mach number contour.

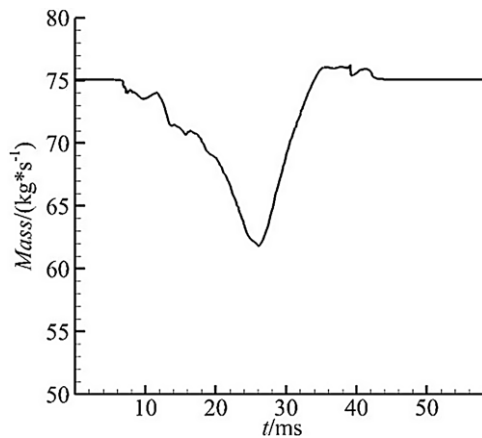


Figure 19. Throat flow history of Case 10.

and 6 with those of Case 3 shows that the maximum depressurisation time in which the inlet can restart increases with the depressurisation range.

When the depressurisation time is too large, the inlet cannot restart (Cases 4 and 6). This is because the final backpressure of the inlet is greater than the pressurisation value from the shock induced by the separation. Therefore, Cases 7 and 8 are set to determine whether the inlet can restart when the backpressure drops continually; the depressurisation speeds here are the same as those for Cases 4 and 6.

Figure 16 shows the throat flow history of Case 7. A buzz starts when the backpressure drops to $13P_0$. Figure 17 shows the throat flow history of Case 8, which is similar to that of Case 7 in which there was a short buzz start when the backpressure dropped to $8P_0$. However, after a period of buzz, the inlet could restart.

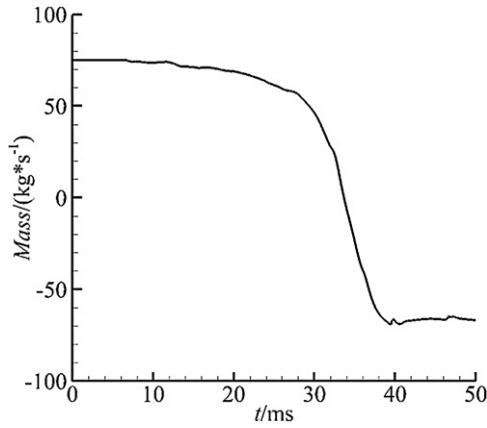


Figure 20. Throat flow history of Case 11.

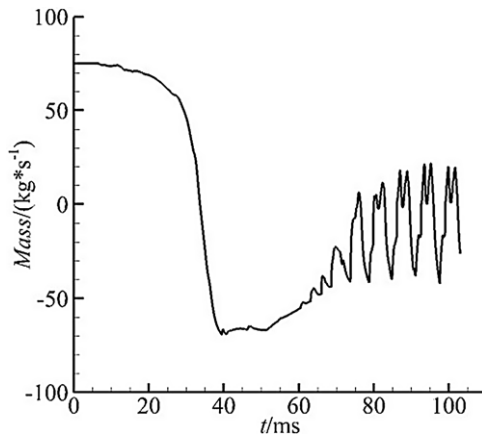


Figure 21. Throat flow history of Case 12.

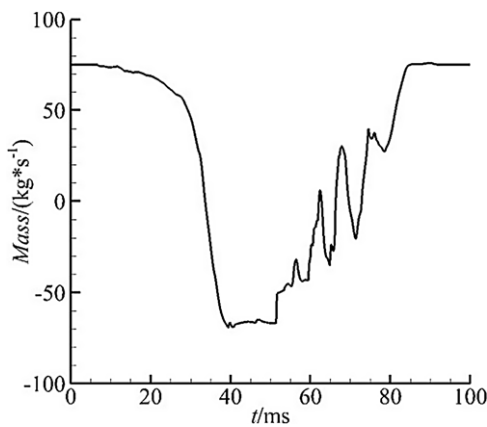


Figure 22. Throat flow history of Case 13.

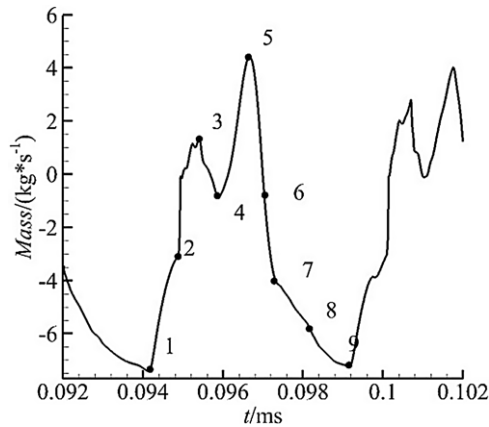


Figure 23. Instantaneous mass flow of the inlet throat for one buzz in Case 7.

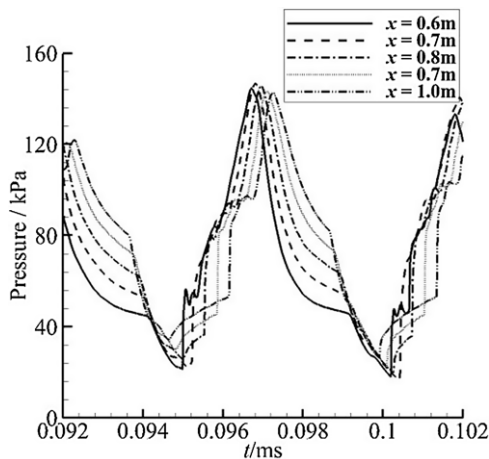


Figure 24. Pressure histories of different points in the diffuser during one buzz for Case 7.

3.2 Unstart and restart characteristics of an inlet under start incoming flow condition

To examine the effects of the depressurisation time and depressurisation value on the inlet unstart and restart characteristics under the start incoming flow condition, we performed simulations with five backpressure variation modes (see Table 3), where $P_0 = 54048$ Pa. Similar to the previous research methods, the unstart flow field of the inlet was simulated first. Then, the depressurisation processes were conducted.

Figure 18 shows the final unstart Mach number contour of Case 9. In this case, the unstart flow field's characteristics are different from those in Case 1. For example, the number of separation zones in front of the inlet lip, and the λ -type detached shock waves are different.

Figures 19 and 20 show the throat flow history of Cases 10 and 11. The inlet can restart when the depressurisation time is 10ms whereas the inlet remains in the unstart state when the time is 20ms. This feature is similar to the restart characteristics under the design conditions. Figure 21 gives the throat flow history of Case 12. Similarly, a buzz starts when the backpressure drops to a slightly bigger value than the pressurisation value from the normal shock. Figure 22 shows the throat flow history of Case 13. The inlet achieves restart after a period of buzz.

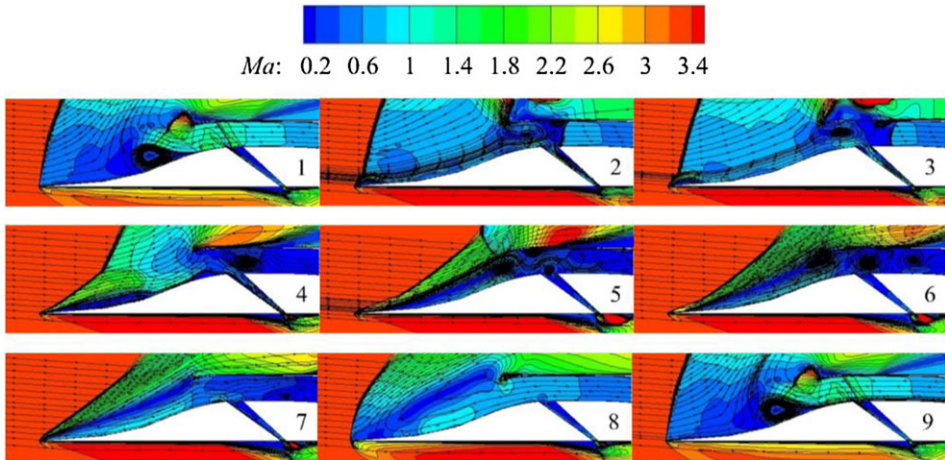


Figure 25. Mach number contours and streamlines for typical points in Fig. 23.

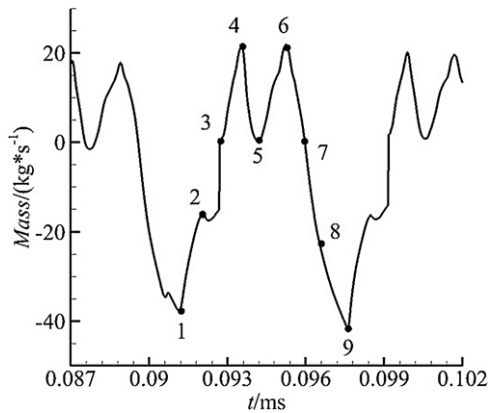


Figure 26. Instantaneous mass flow of the inlet throat during one buzz for Case 12.

According to the earlier investigations, the inlet can restart by increasing the depressurisation range when the big buzz occurs. The final backpressure value is lower than the pressurisation value from the normal shock in a certain incoming Mach number, such as the end value in Cases 8 and 13.

3.3 Inlet buzz

The unstart flowfield is invariably accompanied by buzz; therefore, the buzz flowfields are further investigated to obtain deeper insights into the buzz under such instantaneous backpressure change. Figure 23 shows the instantaneous mass flow at the inlet throat during a buzz for Case 7. Figure 24 shows the pressure histories of different points in the diffuser. Figure 25 shows the Mach number contours and streamlines of the typical points shown in Fig. 23. From these results, the buzz cycle can be categorised into two phases.

In Phase 1 (from point 1 to point 5), the pressure inside the inlet diffuser is sufficiently low because of the long-time reverse flow; therefore, the shock moves downstream, and the inlet swallows the old separated area. Therefore, the incoming mass flow and the pressure in the diffuser increase. At the same

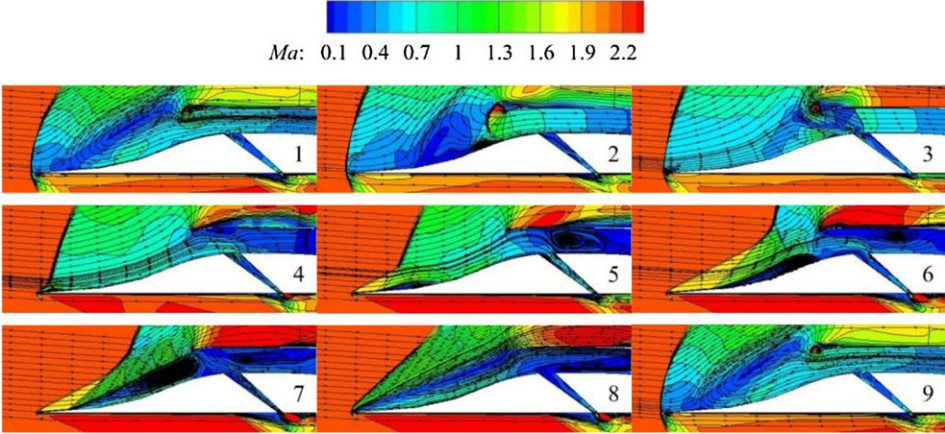


Figure 27. Mach number contour and streamlines for typical points in Fig. 26.

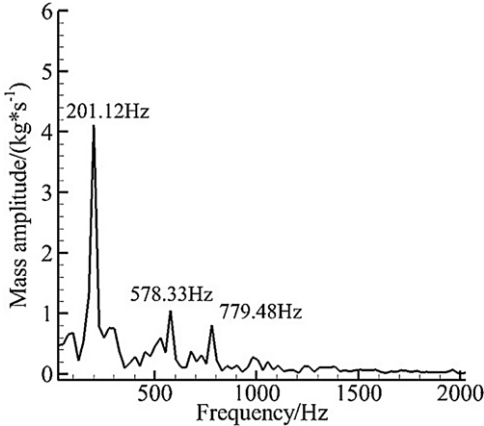


Figure 28. The frequency spectrum of throat mass for Case 7.

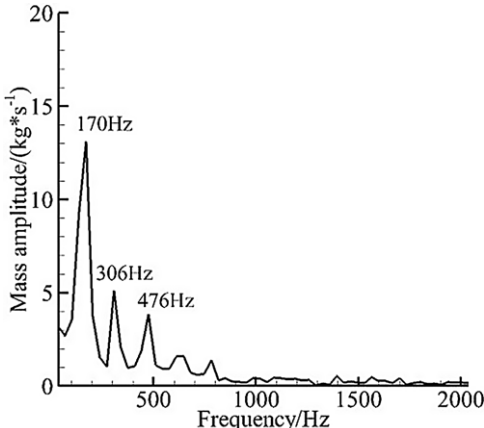


Figure 29. The frequency spectrum of throat mass for Case 12.

Table 4. Base frequencies of the buzz obtained using the formula and simulation

Case	7	12
Freestream Mach number	3.3	2.4
Sound speed (m/s)	822	473
Average Mach number	0.31	0.24
Base frequency of acoustic resonance mode (Hz)	157.42	94.4
Base frequency obtained by numerical simulation (Hz)	201.2	170

time, a new separation develops at the shock foot. The separated area increases as the shock wave move downstream until it occupies all the compression ramps.

In Phase 2 (from point 5 to point 9), the oblique shock moves upstream because of the high pressure inside the inlet. Consequently, airflow spillage increases, and the mass flow rate decreases to zero (point 7); then, a reverse flow occurs. The oblique shock wave angle increases gradually because of the increase in the reverse flow. Simultaneously, the downstream pressure decreases and a newly separated area forms by the interaction of the incoming flow and the reverse flow (point 9), identical to point 1. Then, a new buzz cycle begins.

Similar buzz flows were found in Case 12. The motion of the normal shock and the large separation on the compression ramps are shown in Figs. 26 and 27. The inlet buzz was accompanied by the separation variations at the shock foot.

The buzz mechanism can be classified as Dailey-type buzz [20] in which the buzz is triggered by the obstruction caused by the separation on the compression surface. The minor difference between the two kinds of buzz waves is that the reflux time of Case 7 is longer than that of Case 12. Also, the large separated area formed by the interaction of the incoming flow and the reverse flow is generated only for Case 7. These differences might have resulted from the different boundary conditions.

Figures 28 and 29 show the frequency spectrum results for the throat mass for Case 7 and 12. The main frequencies of the inlet buzz were 201.12Hz for Case 7 and 170Hz for Case 12. The fundamental acoustic modes for a duct with open and closed ends are estimated as follows [21]:

$$f = (2n + 1) \frac{c(1 - (Ma)^2)}{4L} \quad n = 0, 1, 2, \dots, \quad (3)$$

where L ($=1.18\text{m}$) denotes the distance between the cowl lip and inlet out. Ma is the average Mach number of the diffuser, and c is the speed of sound. The simulation results showed that the mean Ma values were 0.31 for Case 7 and 0.24 for Case 12, and the mean c values were 822m/s for Case 7 and 473m/s for Case 12. The calculated fundamental frequencies were 157.42Hz for Case 7 and 86Hz for Case 12. Compared with the frequency spectrum results, the fundamental frequencies of the acoustic resonance modes were less than the base frequencies obtained by simulations (see Table 4). Other studies observed similar phenomena [4, 10, 22]. We inferred that the disturbances that originated from the separation bubble made the base frequency different from the acoustic resonance of the inlet duct.

4.0 Conclusions

This research investigated the unstart and restart characteristics of a two-dimensional supersonic inlet with abrupt backpressure variations. Using thirteen modes of backpressure changes, we reached the following conclusions. The main conclusions are as follows:

The flow field characteristics under the typical unstart phenomenon have two aspects: (i) a decrease in the effective cross-section area of the throat, and (ii) the flow spillage in front of the lip. Consequently, the backpressure-resistance ability of the inlet decreases. As the backpressure rapidly falls to the value

of the normal working state, the inlet can restart; otherwise, the detached shock wave located in front of the lip is pushed upstream until a detached bow shock forms in front of the compression ramps. Then, the inlet sinks into a deep unstart even though the backpressure is close to the normal working value.

Comparing the results obtained from the different depressurisation modes, we found that when depressurisation time is short, it is easier for the inlet to restart at the same depressurisation value. When the depressurisation value is high, the maximum depressurisation time of the inlet takes longer to restart. However, a big buzz generates if the depressurisation time is too long. With the continuing reduction in the backpressure to a low value, the inlet in the deep unstart state can restart after a buzz period. The backpressure value is lower than the pressurisation value from the normal shock for a certain incoming Mach number; otherwise, the inlet enters a long buzz state.

The separation bubble that develops at the shock foot on the compression ramps is mainly responsible for the appearance of a big buzz; this bubble also plays an important role in determining the basic frequency of the buzz.

Acknowledgements. This work is supported by the National Natural Science Foundation of China (Nos. 51906104, 12025202, U20A2070), National Science and Technology Major Project (2019-II-0014-0035), Natural Science Foundation of Jiangsu province (BK20190385), Jiangsu provincial 333 high-level talent cultivation project (Grant No: BRA2018031), the special scientific research project for commercial aircraft, the 1912 project (Grant No. 2019-JCJQ-DA-001-067), the priority academic program development of Jiangsu higher education institutions.

References

- [1] Takasake S., Brett J.C., Fujimoto A., et al. Inlet unstart influence on aerodynamic characteristics of next generation supersonic transport (SST), AIAA Paper, 1998, pp 98–5546.
- [2] Emami S., Trexler C.A., Auslender H., et al. Experimental investigation of inlet combustor isolators for a dual mode scramjet at a Mach number of 4, NASA TP 3502, 1995.
- [3] Van Wie D.M., Kwok F.T. and Walsh R.F. Starting in characteristics of supersonic inlet, AIAA Paper, 1996, pp 1996–2914.
- [4] Rodi P.E., Emami S. and Trexler C.A. Unsteady pressure behavior in a ramjet/scramjet inlet, *J. Propul. Power*, 1996, **12**, (3), pp 486–493.
- [5] Wagner J.L., Valdivia A., Yuceil K.B., et al. An experimental investigation of supersonic inlet unstart, 37th AIAA Fluid Dynamics Conference and Exhibit, Miami, FL, June 2007.
- [6] Mayer D.W. and Paynter G.C. Prediction of supersonic inlet unstart caused by freestream disturbances, *AIAA J*, 1995, **33**, (2), pp 266–275.
- [7] Mayer D.W. and Paynter G.C. Boundary conditions for unsteady supersonic inlet analyses, *AIAA J.*, 1994, **32**, (6), pp 1200–1206.
- [8] Trapier S., Duveau P. and Deck S. Experimental study of supersonic inlet buzz, *AIAA J*, 2006, **44**, (10), pp 2354–2365.
- [9] Trapier S., Duveau P. and Guillen P. Delayed detached-eddy simulation of supersonic inlet buzz, 37th AIAA Fluid Dynamics Conference and Exhibit, Miami, FL, June 2007.
- [10] Trapier S., Deck S. and Duveau P. Time-frequency analysis and detection of supersonic inlet buzz, *AIAA J*, 2007, **45**, (9), pp 2273–2284.
- [11] Li, L., Tan, H.J., Sun, S., et al. Signal characteristics and prediction of unstarting process for two-dimensional hypersonic inlet, *Acta Aeronautica et Astronautica Sinica*, **2010**, **31**, (12), pp 2324–2331.
- [12] Lee H.J., Lee B.J., Kim S.D., et al. Flow characteristics of small-sized supersonic inlets, *Journal of Propulsion and Power*, 2011, **27**, (2), pp 306–318.
- [13] Wooram H. and Chongam K. Computational study on hysteretic inlet buzz characteristics under varying mass flow condition, *AIAA J*, 2014, **52**, (7), pp 1357–1373.
- [14] Xie, L.R. and Guo, R.W. Investigation of restart performance of a mixed-compression two-dimensional supersonic inlet with fixed-geometry, *J Aerosp Power*, 2008, **23**, (2), pp 389–395.
- [15] Chen, Y. *The start characteristic of supersonic inlet*, Xian, Institute of Aerospace Power Technology, 2016.
- [16] Tan, H.J., Sun, S. and Yin, Z. Oscillatory flows of rectangular hypersonic inlet unstart caused by downstream massflow choking, *J. Propul. Power*, 2009, **25**, (1), pp 138–147.
- [17] Meng, Y., Zhu, S., Yan, X. Shock wave oscillation for outlet-closed ramjet inlet, *Journal of Propulsion Technology*, 2011, **32**, (5), pp 606–610.
- [18] Nagashima, T., Obokata, T. and Asanuma, T. *Experimental of Supersonic Air Intake Buzz*, Institute of Space and Aeronautical Science of Tokyo, 1972.
- [19] Neophyton, A., Mastorakos, E. and Cant, R.S. DNS of spark ignition and edge flame propagation in turbulent droplet-laden mixing layer, *Combustion & Flame*, 2010, **157**, (6), pp 1071–1086.
- [20] Dailey, C.L. Supersonic diffuser instability Ph.D. Thesis, California Inst. Of Technology, Pasadena, CA, 1954.

- [21] Newsome, R.W. Numerical simulation of near-critical and unsteady, Subcritical Inlet Flow, *AIAA J*, 1984, **22**, (10), pp 1375–1379.
- [22] Hawkins, W.R. and Marquart, E.J. Two-dimensional generic inlet unstart detection at Mach 2.5-5.0, *AIAA Paper*, 1995, pp 1995–6019.